Methane and carbon dioxide emissions from thermokarst lakes on mineral soils

Alex Matveev, Isabelle Laurion, and Warwick F. Vincent

A. Matveev and W.F. Vincent. Centre d'études nordiques (CEN) & Département de biologie, Université Laval, Québec, Canada

I. Laurion. Institut national de la recherche scientifique, Centre Eau Terre Environnement (INRS-ETE) and Centre d'études nordiques (CEN), Québec, Canada

Corresponding author: Alex Matveev (e-mail: alex.matveev.1@ulaval.ca).

Abstract: Thermokarst lakes are known to emit methane (CH_4) and carbon dioxide (CO_2), but little attention has been given to those formed from the thawing and collapse of lithalsas, ice-rich mineral soil mounds that occur in permafrost landscapes. The present study was undertaken to assess greenhouse gas stocks and fluxes in eight lithalsa lakes across a 200-km gradient of permafrost degradation in subarctic Québec. The northernmost lakes varied in their surface-water CO_2 content, from below to above saturation, but the southern lakes in this gradient had much higher surface concentrations that were well above air-equilibrium. Surface-water CH_4 concentrations were at least an order of magnitude above air-equilibrium values at all sites, and the diffusive fluxes of both gases increased from north to south. Methane oxidation in the surface waters from a northern lake was only 10% of the emission rate, but at the southern end it was around 60% of the efflux to the atmosphere, indicating that methanotrophy can play a substantive role in reducing net emissions. Overall, our observations show that lithalsa lakes can begin emitting CH_4 and CO_2 soon after they form, with effluxes of both gases that persist and increase as the permafrost continues to warm and erode.

Key words: lithalsa, methane, permafrost, subarctic, thermokarst

Introduction

Lakes and ponds in permafrost landscapes are known to be emission sources of greenhouse gases (GHG) to the atmosphere (Tan and Zhuang 2015; Holgerson and Raymond 2016), with potentially large feedback effects on global climate (Grosse et al. 2016; Kokelj and Jorgenson 2013). Zimov et al. (1997) drew attention to the strong output of CH_4 from lakes in Siberia formed by thawing and collapse of ice-rich permafrost (thermokarst), and concluded that the CH_4 was largely derived from ancient organic carbon that had been previously stored in the frozen soils. Subsequent research suggested that this process may have accelerated the deglaciation during the early Holocene (Walter et al. 2007). A synthesis of data from boreal and Arctic lakes noted that two thirds of the total CH_4 emissions from landscapes north of latitude 50°N is derived from freshwater systems, with thermokarst lakes contributing about 25% of that total (Wik et al. 2016). A constraint in defining the error in such estimates, however, is the poorly known extent of local and regional variability in GHG fluxes, with large variations among thermokarst lakes (Laurion et al. 2010; Sepulveda-Jauregui et al. 2015; Vonk et al. 2015).

Another major source of variability in GHG emissions from thermokarst lakes is that associated with landscape evolution (Allan et al. 2014; Grosse et al. 2016; He et al. 2012; Lipson et al. 2015). Fluxes of CH_4 to the atmosphere are thought to be especially high in newly degrading permafrost soils (Kanevskiy et al. 2014; Elvert et al. 2016), with older lakes succumbing to drainage (Grosse at al. 2013; van Huissteden et al. 2011), thereby eliminating the habitat for aquatic methanogens. Thermokarst lakes can also be subject to infilling by sediment and fen/bog vegetation, which may cause such lakes to become net sinks of carbon (Payette et al. 2004; Bouchard et al. 2016). However, the exact trajectory of geomorphological change and the

54 associated biogeochemical effects remain uncertain in many regions of permafrost thaw and
55 degradation.

56 In the subarctic region of northern Québec, Canada, two types of landscape contain
57 permafrost mounds and associated thermokarst lakes (Allard and Seguin 1987). First, palsa
58 landscapes occur in organic-rich peatlands, with uplifted ice-cored mounds of frozen *Sphagnum*
59 and thermokarst lakes created by their permafrost thawing and collapse. The thermokarst lakes
60 associated with palsas (hereafter, palsa lakes) are typically dark-coloured because of elevated
61 concentrations of coloured dissolved organic matter (CDOM). Sunlight is strongly absorbed in
62 their near-surface waters, and the lakes are highly stratified with anoxic conditions through most
63 of the water column and during most of the year (Deshpande et al. 2017). These low or zero
64 oxygen (O_2) environments are conducive to methanogenesis, and palsa lakes have strong
65 emissions of both CH_4 and CO_2 to the atmosphere (Matveev et al. 2016). Another type of terrain
66 occurs on mineral soils as lithalsa landscapes (Calmels et al. 2008), with frost-heaved, clayey,
67 silt-rich permafrost mounds and associated thermokarst lakes (hereafter, lithalsa lakes). Lithalsa
68 lakes are more varied in colour, from blue-green to white to brown (Watanabe et al. 2011), and
69 are also known for their stratified structure and anoxic bottom waters (Deshpande et al. 2015).
70 Like palsa lakes, they accumulate CH_4 and CO_2 (Laurion et al. 2010) and have high rates of
71 bacterial heterotrophic production (Breton et al. 2009; Roiha et al. 2015).

72 The aim of the present study was to provide an improved understanding of GHG stocks
73 (specifically CO_2 and CH_4) in lithalsa lakes, and of the emission fluxes from such lakes at
74 different stages of permafrost degradation. We hypothesized that stocks and emissions increase
75 with increasing degree of permafrost degradation, with greatest effects at the warm southern
76 margin of Arctic permafrost landscapes. This hypothesis implies that the northward contraction of
77 permafrost will be accompanied by increased rates of emission, which could continue well after

lake formation. We evaluated this hypothesis by making measurements at a series of lithalsa lakes across a gradient of permafrost conditions in subarctic Québec, including at the southern limit of current permafrost extent where thermokarst lakes have formed and persisted for at least many decades.

Materials and methods

Study sites

Sampling was in the western Hudson Bay area of Nunavik (Northern Quebec, Canada; Fig. 1), a region experiencing rapid warming and landscape change (Bhiry et al. 2011), and the location of multiple research sites within the program 'Arctic Development and Adaptation to Permafrost in Transition' (ADAPT; Vincent et al. 2017) that this study was part of. The region spans four different permafrost zones, from continuous and discontinuous widespread permafrost in the north, to sporadic and isolated permafrost in the south (Allard and Seguin, 1987 Vallée and Payette 2007), with mean annual air temperatures over that geographical range from –4.7 to –2.8 ºC. Sampling of lithalsa lakes was at three sites across this north-south gradient (Fig. 1): (a) in discontinuous widespread permafrost, north of the Nastapoka River (56.9°N, 76.3°W; NAS lakes); (b) in discontinuous permafrost, 20 km east of the village of Umiujaq (56.6°N, 76.2°W; BGR lakes); and (c) in degraded sporadic permafrost, 13 km north of the village of Whapmagoostui-Kuujjuarapik and around 200 km south of the NAS site (55.2°N, 77.5°W; KWK lakes; Fig. S1 and associated video[1]; additional descriptions are given in Bégin and Vincent 2017).

[1] Supplementary data are available with the article through the journal website.

98

99 **Lake sampling and physical, chemical and biological properties**

100 In situ measurements and samples were collected from 8 lakes at the three sites (Fig. 1,
101 Table S1[1]) during the summer open-water period, from 2012 to 2015. Vertical profiles of
102 physicochemical properties were obtained from an inflatable boat transported to the sites by
103 helicopter, with a YSI 6000 multi-probe (Yellow Springs Instruments, Yellow Springs, OH,
104 U.S.A.) and an RBR Concerto conductivity-temperature-depth logger (RBR Ltd., Ottawa, ON,
105 Canada). The accuracy of these measurements was ±0.15 °C, ±0.2 pH units, ±0.2 mg oxygen L^{-1},
106 and ±0.001 mS cm^{-1} conductivity for the YSI; and ±0.002 °C and ±0.003 mS cm^{-1} for the RBR.
107 Underwater photosynthetically active radiation (PAR) irradiance was measured with a Licor
108 submersible radiometer.

109 Samples for water analysis were collected at the surface and bottom of the water
110 column, filtered at the Centre for Northern Studies (CEN) research station in Whapmagoostui-
111 Kuujjuarapik, and then shipped to home facilities (Laval University and INRS, Quebec City,
112 Canada) for laboratory analysis. Samples for analysis of soluble reactive phosphorus (SRP) were
113 filtered through 0.2 μm cellulose acetate filters and then analyzed using a colorimetric method
114 (Standard Methods 4500-P.E., APHA, AWWA, and WEF 1998) and a Lachat Autoanalyzer
115 (Lachat QuikChem® 8500 Series 2 Flow Injection Analysis System, Hach Company, Loveland,
116 CO, USA). For total phosphorus (TP), unfiltered samples were acidified with 15% H2SO4,
117 digested with persulfate and analyzed for SRP as above. For dissolved organic carbon (DOC)
118 concentrations, filtered (as above) lake water samples were acidified to remove inorganic carbon,
119 and analyzed by high temperature catalytic combustion method with infrared detection (Standard

[1] Supplementary data are available with the article through the journal website.

120 Methods 5310 B, APHA, AWWA, and WEF 1998) in a Shimadzu VCPH analyzer (Shimadzu
121 Scientific Instruments, Columbia, MD, USA). The total nitrogen content (TN) was measured
122 from unfiltered water samples by alkaline digestion with persulfate, followed by analysis by the
123 sulfanilamide colorimetric method after reduction with cadmium in a Lachat Autoanalyzer
124 (QuikChem® Method 10–107-04-3-A). Total suspended solids (TSS) were determined by weight
125 after filtration onto precombusted, preweighed glass fiber filters (nominal porosity of 0.7 μm).
126 chlorophyll *a* concentration (Chl-*a*) was measured by high-pressure liquid chromatography from
127 pigments extracted with 95% MeOH from the above glass fiber filters kept frozen at −80 °C until
128 analysis, as in Bonilla et al. (2005).

129

130 **Automated lake surface observations**

131 Automated cameras (Reconyx PC800, Holmen, WI, U.S.A.) were installed on the shores
132 of three thermokarst lakes (one per study site, respectively KWK12, BGR1 and NASa) at a
133 distance of 5–10 m from the edge of the summer water extent. The cameras recorded 6
134 photographs per 24 h period at 1-hour intervals, between 10:00 and 15:00 (Eastern Standard
135 Time, EST). The data were retrieved annually, at the end of August each year. The complete
136 dataset is archived in the Nordicana D data repository (Pienitz et al. 2017). These data were used
137 to calculate the number of days of open water for each site, including for the gas flux
138 calculations.

139

140 **CH_4 and CO_2 measurements**

141 Profiles of CH_4 and CO_2 concentrations were obtained from discrete depth samples, as in
142 Deshpande et al. (2017), and with continuous automated dissolved gas monitoring systems. The
143 discrete depth samples were obtained in triplicate with a thin-layer laminar-flow sampler that had
144 two plates set 63.5 mm apart (Matveev et al. 2016), at 0.1 to 0.5 m depth intervals. The samples
145 were transferred with a peristaltic pump to a 2 L pre-rinsed LDPE bottle. The lake water was then
146 equilibrated with a 20 mL air-filled headspace, and a 10 mL gas sample taken and injected into a
147 5.9 mL helium-flushed, evacuated borosilicate glass vial (Labco Exetainer®, Labco Limited, UK).
148 The gas samples were subsequently analyzed for CH_4 and CO_2 by gas chromatography with
149 flame ionization detection (Varian 3800, COMBI PAL head space injection system, CP-Poraplot
150 Q 25m with flame ionization detector) as in Matveev et al. (2016).

151 The surface fluxes of CH_4 and CO_2 were calculated from the dissolved gas concentrations
152 at the air-water interface as in Matveev et al. (2016). We used a wind-based model, with
153 correction for turbulence and low solubility gases as in Vachon et al. (2010). The gas flux F_i for
154 each gas *i* was expressed assuming molecular diffusion, as:

155 $$F_i = k_i \, K_{Hi} \, \Delta P_i \qquad (1),$$

156 where K_{Hi} is the Henry Law constant, k_i is the gas transfer velocity, and ΔP_i is the gradient of the
157 gas partial pressures at the air-water interface.

158 Two automated systems were used, depending on sampling conditions: (1) a 'CO_2-box'
159 continuous GHG monitoring system that simultaneously measured dissolved CO_2, CH_4 and O_2
160 content in a gas stream continuously equilibrated with the source water (Carignan 1998, details in
161 Laurion et al. 2010); and (2) a Franatech METS system composed of an infrared-CO_2 sensor and
162 a semi-conductor CH_4 sensor (Franatech GmbH, Lüneburg Germany) in separate housings and

assembled on a flow-through chamber with a constant water flow produced with a submersible pump (model SBE-5T, Sea-Bird Electronics, Inc., Bellevue, WA, USA). The two instruments were cross-calibrated and the datasets combined (an example of the consistency among methods is given in Fig. S2[1]).

Gas concentrations in the littoral zone were measured with the CO_2-box deployed from the shore (KWK12, BGR1), while concentrations in the deepest offshore water and for the NASa transect were measured with the Franatech METS instrument deployed from the boat. The intake of the CO_2-box was submerged to 5–10 cm from the surface, with the peristaltic pump located inside the instrument housing; the METS intake was a 15 cm tube connected to a submersible Seabird pump, and the entire instrument was submerged at around 10 cm depth from the surface for surface samples.

Ebullition of CH_4 and CO_2 was assessed at KWK and BGR sites by collecting gas samples with submerged, opaque, inverted cones, with a 0.5 m^2 opening at the bottom and a syringe equipped with a valve at the top (details in Matveev et al. 2016). Two to three gas traps per lake were installed for 1 to 30 days, depending on ebullition rates and logistic constraints. The gas samples were stored in 12 mL or 5.9 mL Labco Exetainer® vials, prepared as above. Sampling dates and numbers of ebullition samples for each lake are given in supplementary Table S2[1], which also provides the sampling dates for dissolved gas concentrations measured by the headspace, CO_2-box and METS profiler methods, as described above.

The CH_4 oxidation rates were calculated as a linear regression from concentrations measured every 3 h by subsampling a closed vessel containing 20 L of surface lake water

[1] Supplementary data are available with the article through the journal website.

connected to the CO_2-box. The incubations were performed in the laboratory under ambient temperature (ca. 15°C) and low light (< 50 µmol photons m^{-2} s^{-1}).

Isotopic composition and radiocarbon

Samples for CO_2 and CH_4 radiocarbon dating (^{14}C isotope) were collected in helium-flushed, evacuated 50 mL serum bottles (Wheaton, USA) from two gas ebullition samples collected from funnels installed in lake BGR1 in 2014. The ^{14}C content of CO_2 and CH_4 was measured by accelerator mass spectrometry in the Keck Carbon Cycle AMS Facility of the University of California Irvine (CA, USA), as in Matveev et al. (2016). The ^{14}C ages were expressed as fractions of the modern standard ($\Delta^{14}C$) following Stuiver and Polach (1977), with all results corrected for isotopic fractionation.

The $\delta^{13}C$ isotopic fractionation was assessed in the ebullition and the discrete depth samples, all collected in triplicates by the headspace method and stored in 12 mL Exetainer® vials, prepared as above. The $\delta^{13}C$ in CH_4 and CO_2 was measured at the GRIL-UQAM facility (Montreal, QC, Canada) by continuous-flow Cavity Ring-Down Spectroscopy (CRDS) with near-infrared laser source method, using a Picarro (Picarro Inc., Santa Clara, CA, U.S.A.) 'G2201-*i* $\delta^{13}C$ in CH_4 and CO_2 Gas Analyzer' (<0.12 ‰ $\delta^{13}C$-CO_2 and <0.4 ‰ $\delta^{13}C$-CH_4 precision at 1-σ, 1-hour window, 5-minute average). The results were expressed as the $\delta^{13}C$ ratio of a sample relative to the Vienna Pee Dee Belemnite (VPDB) international measurement standard (Coplen 2011). The isotope separation factor between $\delta^{13}C$-CO_2 and $\delta^{13}C$-CH_4 (ε_C) was calculated according to Whiticar (1999):

$$\varepsilon_C = \delta^{13}C\text{-}CO_2 - \delta^{13}C\text{-}CH_4 \quad (2)$$

206 The $\delta^{13}C\text{-}CO_2$ – $\delta^{13}C\text{-}CH_4$ carbon isotope partitioning resulting from microbial CH_4 production
207 and oxidation was further expressed as a combination plot of the $\delta^{13}C\text{-}CO_2$ vs. $\delta^{13}C\text{-}CH_4$, as in
208 Fig. 8 of Whiticar (1999).
209

210 **Results**

211 **Morphometry**

212 The lithalsa lakes were all shallow, with an average (± SD) depth of 2.7 (± 1.1) m (Table
213 S1[1]), and a distinct morphometry with steep, eroded shores (Fig. S2[1]). The maximum depths were
214 relatively stable among sampling years at KWK and NAS from 2012 to 2015, but BGR1
215 increased by 0.6 m to a maximum of 4.4 m, while BGR2 increased by 0.25 m to a maximum of
216 1.55 m. The mean surface area of the studied lakes averaged 942 m^2 with large variations among
217 sites (CV = 94%), but much less between lakes within each site (average CV = 19%). Within this
218 limited data set, the average lake area per site decreased as a function of distance (R^2 = 0.88 for
219 the linear regression) southwards in the study region (Fig. S3, Table S1[1]). There were no
220 observed changes during the period of observation in lake area at KWK and NAS sites, but the
221 BGR site showed further evidence of rapid landscape change. Some of the lithalsa mounds
222 experienced thawing and collapse (thermokarst), producing new lithalsa lakes (e.g., BGR*b*), and
223 there were also increases in area of some lakes (e.g., BGR1, BGR2) and fusing of adjacent water
224 bodies (Fig. 2).
225

[1] Supplementary data are available with the article through the journal website

226 **Ice regime and winter snow accumulation**

227 The automated camera records showed the lakes were ice-covered for around 8 months
228 each year. At the lake NAS*a* (site NAS) the lake ice formed at the beginning of November
229 (2014), with an overlying layer of snow that accumulated to a maximum thickness of 0.8 m
230 (winter 2015). The ice first broke up during the last week of April (2015), but quickly reformed,
231 with final break-up and disappearance during the first two weeks of June (2015). At the BGR site,
232 the lake ice broke up on lake BGR1 during the last week of May (2015), and the open water
233 period extended from the first week of June until the second week of October (2016). The
234 maximum winter snow accumulation was around 0.7 m (winter 2016). The ice-free period
235 recorded at the lake KWK12 (in the southern KWK valley) was about 2 weeks longer than in
236 BGR (from the last week of May to the third week of October 2016), with a maximum winter
237 (2016) snow accumulation of ca. 0.6 m. None of the three lake ice records showed any evidence
238 of persistent gas bubbling ('bubbling hot-spots' as in Wik et al. 2011) on images with clear ice
239 during its formation and break-up.

240

241 **Limnological properties**

242 All of the lithalsa lakes were thermally stratified during the period of observation, with the
243 shallowest thermocline occurring at 0.5 m depth in NAS*a* (Fig. 3a), possibly linked to the strong
244 light attenuation in its turbid waters (surface TSS = 319 mg L^{-1}, Table 1). The surface mixing
245 zone was 2 and 1.5 m deep in the lakes BGR1 and KWK12 respectively (Fig. 3d, g). The depth of
246 the euphotic zone (1% of surface PAR) similarly varied among the lakes, from 0.55 m in NAS*a*
247 to 4.1 m (to the lake bottom) in BGR1 (Fig. 3a, d, g). The pH was close to neutral in most lakes
248 of NAS and BGR sites (Fig. 3b, e), while it was significantly lower in KWK lakes ($P<0.0001$ in

2-way ANOVA per site comparison), falling to acidic values of 4.6 at the bottom of KWK12 (Fig. 3h). Specific conductivity values varied from 2.7 to <15 mS m^{-1} in most lakes of different permafrost regions, typically increasing with depth by about 50% (Fig. 3b, h), with the exception of BGR1, where it sharply increased up to 40.1 mS m^{-1} below the mixing zone (Fig 3d, e).

TN and TP concentrations were variable among lakes in all sites (Table 1), with no significant difference between the top and bottom of the water column ($p>0.1$, Wilcoxon test). SRP averaged high values (3.5 µg P L^{-1}), but was similarly variable in all lakes (CV = 85 %), and with no significant difference between the top and bottom of the water column ($p=0.12$, Wilcoxon test). The lakes had substantial concentrations of TSS in their bottom waters, with exceptionally high values throughout the water column of NAS*a* (Table 1). DOC concentrations (all depths combined) were significantly higher ($p = 0.007$, t-test) in the southern KWK lakes versus northern lakes (BGR and NAS, Table 1), averaging 14.5 and 4.9 mg C L^{-1}, respectively. Chl-*a* concentrations (all depths combined) were also significantly higher ($p=0.025$, t-test) in the southern (mean of 16.9 µg L^{-1}) versus northern (mean of 2.5 µg L^{-1}) lakes.

Dissolved gas concentrations

Dissolved O_2 concentrations were typically at saturation at the surface of all lakes, with undersaturation at depth, while CH_4 and CO_2 concentrations varied considerably among sites, lakes and lake depths (Fig. 4). CO_2 concentrations increased toward the bottom in all lakes. CH_4 concentrations also increased with depth in KWK and BGR lakes (Fig.4c-f), but were similar throughout the water column in NAS lakes (Figs 4a, b).

Unlike other lakes, the surface waters of lake NAS*a* were undersaturated in CO_2 to the depth of 1 m (Fig. 4a) and this gas was in low concentration to 3 m in NAS*h* (Fig. 4b). In lakes of the BGR site, surface CO_2 values varied from 29.9 µmol L^{-1} in BGR1 and 20.5 µmol L^{-1} in

273 BGR2, to 42.5 μmol L^{-1} in the newly formed lake BGR*b* (Table 2). All these were above the air
274 equilibrium value of about 16.7 μmol L^{-1} (Fig. 5). Surface CO_2 concentrations were less variable
275 and generally higher in KWK lakes relative to those in the north, averaging 45.4 ±13.2 μmol L^{-1}.
276 The CH_4 concentration at the surface of NAS lakes varied from 0.027 to 0.21 μmol L^{-1} (Table 2),
277 all at least an order of magnitude above the air equilibrium value of about 0.0031 μmol L^{-1} (Fig.
278 5). The CH_4 concentrations in BGR lakes were much higher, from 0.35 to 0.80 μmol L^{-1} (Fig. 4c,
279 d), and averaged 0.41 μmol L^{-1} (Table 2). KWK lakes also had high surface CH_4 concentrations
280 averaging 0.43 μmol L^{-1}, including the highest encountered in this study, and large variability
281 among lakes (CV = 78%).

282 The bottom waters of all lakes were supersaturated in CH_4 and CO_2, with concentrations
283 2-3 orders of magnitude higher than at the surface (Fig. 4, 5). The vertical gradients were much
284 steeper in KWK lakes compared to those in NAS lakes and in some of the BGR lakes (Fig.4);
285 BGR1 (Fig. 4c) and the newly formed BGR*b* (Fig. S4[1]) also had steep gradients in CO_2 and CH_4
286 concentrations towards the bottom. The bottom concentrations of CH_4 and CO_2 were 1 or more
287 orders of magnitude higher in the lakes of the southern KWK site (mean ±SD: 1259 ±1066 μmol
288 CO_2 L^{-1}, 310 ±281 μmol CH_4 L^{-1}) relative to those of the northernmost NAS site (120 ±58 μmol
289 CO_2 L^{-1}, 0.14 ±0.08 μmol CH_4 L^{-1}). Values at the BGR sites (1081 ±1402 CO_2 L^{-1}, 162 ±165
290 μmol CH_4 L^{-1}) were similar to or below those at KWK, however the lake-to-lake variability at all
291 sites was considerable, as shown by the large SD values.

292 To examine lateral variations in GHG concentrations, we sampled one of the larger lakes
293 (NAS*a*) in duplicate at the surface and below the surface (0.7 to 1.0 m depth) at 5 stations
294 extending from one side of the lake to the other (Fig. 6). The variation in CH_4 concentrations was

[1] Supplementary data are available with the article through the journal website.

295 small, with CVs of 8 % (surface) and 9 % (subsurface). The CO_2 variation was slightly larger,
296 with CVs of 23 % (surface) and 20 % (subsurface), with the lowest concentrations measured in
297 the littoral zone at each end of the transect.
298
299 **CH_4 and CO_2 fluxes**

300 The diffusive CO_2 flux from Nunavik lithalsa lakes gradually increased towards the south
301 in the region of study (Table 3). The values ranged from a net sink of –1.7 mmol CO_2 m^{-2} d^{-1} (in
302 lake NAS*a*) to a source of up to 30.8 mmol CO_2 m^{-2} d^{-1} in lake KWK12 (Table 4), with an
303 intermediate value of 8.1 ±7.7 mmol CO_2 m^{-2} d^{-1} on average in BGR lakes. Although the CO_2
304 flux at NAS was on average negative, it alternated between positive and negative values both
305 within one lake and between the lakes of this site at different visits (CV = 168%). The average
306 diffusive flux of CO_2 from the southern KWK lakes (20.2 ±7.1 mmol CO_2 m^{-2} d^{-1}) was more than
307 double that from BGR, and an order of magnitude greater than from NAS lakes. There was no
308 significant correlation between the concentrations of DOC and CO_2 in these lakes (Table 1; r =
309 0.33, p = 0.42 for surface waters; r = 0.63, p = 0.2 for bottom waters). The diffusive CO_2 fluxes
310 were several orders of magnitude greater than the CO_2 ebullition fluxes, the latter only measured
311 in BGR and KWK lakes (Table 3). However, the CO_2 ebullition flux was an order of magnitude
312 greater at the BGR site (0.01 mmol CO_2 m^{-2} d^{-1}) relative to KWK (0.006 mmol CO_2 m^{-2} d^{-1}).

313 The positive southward gradient was also observed in the CH_4 diffusion rates from these
314 Nunavik lithalsa lakes (Table 3). The diffusive CH_4 fluxes at the NAS site were always positive
315 (0.12 ±0.03 mmol m^{-2} d^{-1}), and with low variability between the lakes (CV = 25%). Diffusive
316 emissions from BGR lakes averaged 0.45 ±0.06 mmol CH_4 m^{-2} d^{-1}, in the same order of
317 magnitude than from KWK lakes that showed greater variability (0.47 ±0.33 mmol CH_4 m^{-2} d^{-1}).

Similar to the observations for CO_2, the mean CH_4 ebullition from the BGR site on discontinuous permafrost (0.26 mmol CH_4 m^{-2} d^{-1}) was an order of magnitude greater than that from the KWK site in the largely degraded isolated permafrost region (0.016 mmol CH_4 m^{-2} d^{-1}). Overall, the observed total CH_4 fluxes from the studied lakes were within the range of values observed in other thermokarst lakes in the circumpolar region, and the CO_2 fluxes were at the upper limit or above the values reported elsewhere (Table 4).

Isotopic fractionation and ^{14}C-dating of greenhouse gases

In general, the $\delta^{13}C$ isotopic signatures in dissolved gases were similar in surface waters of the lithalsa lakes (Table 5), with the exception of a low $\delta^{13}C$-CH_4 value in the surface water of newly formed lake BGR*b*. The bottom water $\delta^{13}C$ signatures differed significantly from those at the surface in KWK lakes for $\delta^{13}C$-CH_4 (paired t = 5.8, p = 0.01**)** but not for $\delta^{13}C$-CO_2 (paired t = 2.3, p = 0.07), and for neither gas in the BGR lakes ($\delta^{13}C$-CH_4: paired t = 1.5, p = 0.15; $\delta^{13}C$-CO_2: paired t = 0.6, p = 0.3). There was greater $\delta^{13}C$ depletion in CH_4 relative to CO_2 in all samples, as expected (Table 5). For all lakes, the isotope separation factor between $\delta^{13}C$-CO_2 and $\delta^{13}C$-CH_4 (ε_C) averaged (±SD) -29.1 ±7.1 ‰ in the surface waters, and -40.4 ±6.5 ‰ in the bottom waters (Fig. 7), and there was also a significant difference in ε_C between the surface and bottom waters of KWK lakes (paired t = 5.5, p = 0.03) but not BGR lakes (paired t = 1.1, p = 0.40). The $\delta^{13}C$-CH_4 measured in the single BGR1 ebullition sample was –65.6 ‰, which was more depleted than the lowest dissolved CH_4 value for this lake ($\delta^{13}C$-CH_4 of –55.2 ‰ in the bottom waters).

339 The ^{14}C-age of the ebullition gases collected from lake BGR1 was also highly variable,
340 with the oldest carbon contained in the CO_2. The $\Delta^{14}C$ values measured in the CO_2 in this lake
341 ranged from –225 ±10.6 ‰ to –517.1 ±4.7 ‰, corresponding to the age range from 1990 ±110 to
342 5790 ±80 years before present (yrs. BP) respectively. The $\Delta^{14}C$ values measured in CH_4 in this
343 lake ranged from 34.4 ±17.3 ‰ to 83.7 ±1.8 ‰, corresponding to modern age (100 to 320 yrs.
344 BP).

345

346 **CH_4 oxidation rates**

347 Concentrations of CH_4 during the two laboratory incubations of lake water decreased linearly
348 with time over the 27 to 48 h duration of the experiments, while CO_2 concentrations increased
349 (Fig. 8). These net CH_4 consumption rates were an order of magnitude higher for KWK (0.38 ±
350 0.02 μmol CH_4 L^{-1} d^{-1}, R^2= 0.92) compared to NAS (0.016 ±0.002 μmol CH_4 L^{-1} d^{-1}, R^2= 0.94).
351 These values corresponded to 5.7 % (KWK) and 0.8 % (NAS) of the measured net CO_2
352 production rates.

353

354 **Discussion**

355 Landscape changes in the region of the present study were most evident in the BGR area,
356 with deepening, expansion and fusion of lakes, and the creation of new lakes (Fig 2). These
357 effects of the northward contraction and rapid degradation of permafrost have been well
358 documented at BGR (Calmels et al. 2008). Changes of similar origin and scale were observed in
359 the past at the southern end of our sampling region, the KWK valley site, during the period 1930
360 to 1960 (Allard and Seguin 1987). Over more recent decades, however, the total areal extent of

lithalsa lakes in degraded permafrost region has remained relatively constant (Bouchard et al. 2014). Despite the older age, the KWK lakes continued to retain water up to a depth of almost 3 m, with strong stratification and anoxic bottom layers indicating intense microbial activity.

The diffusion rates of both CO_2 and CH_4 were much greater in the KWK lakes than at the more northerly sites where permafrost was less degraded, particularly relative to the NAS lakes. The rates of high diffusion exceeded those for ebullition at all measured sites. This contrasts with many reports for thermokarst lakes elsewhere, where ebullition was the dominant flux (Casper et al. 2000; Bastviken et al. 2011; Wik et al. 2013; Sepulveda-Jauregui et al. 2015). It remains possible that our limited sampling of ebullition missed important periods and places of intense ebullition, and that the values presented here are underestimates. The largest ebullition fluxes that have been observed elsewhere are persistent point sources ('seeps' and 'hotspots', as in Walter Anthony et al. 2010), which are identifiable in the lake ice-cover (Wik et al. 2011; Lindgren et al. 2016). However, our continuous automated camera imaging of the lake surfaces did not reveal any persistent point ebullition in these lakes, nor were such hotspots observed during the sampling campaigns in four consecutive years. Thus, the undersampling error in our estimates of the ebullition flux seems unlikely to be large. It is possible, however, that our estimates of diffusion flux may have included quasi-stable microbubbles of gas (Prairie and del Giorgio 2013) that form in the supersaturated bottom waters and rise up through the water column (Matveev et al. 2016).

The total CH_4 efflux rates varied among sites and, to a lesser degree, among years and month of sampling, but at all locations the rates were substantial (Table 3). The maximum combined emission rate per unit area of 1.2 g CO_2-eq m^{-2} d^{-1} was observed in the KWK site experiencing accelerated permafrost degradation. However, the larger northernmost lakes of the

384 NAS site were emitting a similar amount of gas per lake, even although only diffusive fluxes
385 were measured there (Table 3). The KWK lithalsa lakes, which lie in the most degraded
386 permafrost region, had minimal ebullition rates (7.2 mg CO_2-eq m^{-2} d^{-1}, versus rates of 2450 mg
387 CO_2-eq m^{-2} d^{-1} for lakes elsewhere reported in Wik et al. 2016), and were the smallest of all the
388 studied lithalsa sites in terms of lake area (Table S1[1]). Despite these features, they still emitted an
389 estimated 72.3 kg CO_2-eq y^{-1}, as high as the recently formed BGR*b*. The camera images also
390 indicated that they had a two-week longer open water period, which would favour a more
391 prolonged period of emission.

392 Although these rates generally fall within the range of emissions reported elsewhere, they
393 are less than those of palsa lakes in the same region (Table 4). Palsa lakes show similar pattern of
394 emissions dominated by diffusion, but their organic-rich nature and intense bacterial activity
395 (Deshpande et al. 2016) creates anoxic conditions through most of the water column (Deshpande
396 et al. 2017), with abundant methanogenic communities (Crevecoeur et al. 2016) and thus high
397 rates of methanogenesis. Even the oxygenated strata of these waters may be sites of
398 methanogenesis, as recorded in oxic environments elsewhere (Bogard et al. 2014), and CH_4
399 production may be favoured by anoxic microenvironments within the organic particles that occur
400 in high concentration in these waters.

401 The gas concentrations and emission rates measured here were made during the summer
402 period of open water, and future studies will need to consider the full annual cycle. Continuous
403 oxygen data from these subarctic waters indicate prolonged anoxia under the winter ice cover,
404 with mixing of the water column that may be delayed until convective overturn in autumn
405 (Deshpande et al. 2015, 2017). Additional CH_4 and CO_2 sampling would therefore be of

[1] Supplementary data are available with the article through the journal website.

406 particular interest during the late winter ice-cover, spring ice-out and fall cooling periods.
407 Variations are also likely at much shorter timescales. The lithalsa lakes contain moderate
408 chlorophyll *a* levels (Table 1), and phytoplankton as well as aquatic macrophytes may cause
409 diurnal fluctuations in O_2, CO_2 and possibly also CH_4. Previous studies with the CO_2-box on the
410 KWK lakes, for example, have provided initial indications of such diurnal cycles in all three
411 gases (see Fig. 7c in Laurion et al. 2011). Nocturnal cooling and convective mixing may also
412 influence emission rates (Walter Anthony and MacIntyre 2016).

413

414 **CH_4 oxidation**

415 Our laboratory experiments indicate active methanotrophy taking place in these waters under
416 oxygenated conditions, as was expected from previous 16S RNA analyses showing the presence
417 of abundant methanotrophs in these waters (Crevecoeur et al. 2015). In both the KWK and NAS
418 lakes this contributed a small fraction (around 1 to 6%) of the total microbial respiration rate,
419 consistent with the high rates of bacterial heterotrophy in thermokarst waters (Deshpande et al.
420 2016, Roiha et al. 2016). It is also consistent with the ^{14}C data that showed large differences in
421 age between the two GHG, since CO_2 derived from CH_4 oxidation would yield the same age (see
422 below). The CH_4 oxidation rates (0.016 and 0.38 μmol CH_4 L^{-1} d^{-1} respectively for NAS and
423 KWK lakes) are at the low end of the range reported in other environments, for example 0.02 to
424 1.3 μmol CH_4 L^{-1} d^{-1} in the surface waters of a boreal lake in Finland (Kankaala et al. 2006).
425 Much higher rates (1.2 to 33.8 μmol CH_4 L^{-1} d^{-1}) were reported from Alaskan lakes across a
426 range of landscapes in summer, however these estimates were derived from longer term (10–12
427 d) incubations after CH_4 enrichment (Martinez-Cruz et al. 2015). The CH_4 oxidation rates
428 observed in the present study also imply that methanotrophy in lithalsa lakes is a much slower

loss process than efflux to the atmosphere: the turnover time for CH_4 in KWK12 based on these measured oxidation rates would be 4.4 days, but only 2.8 days based on emission to the atmosphere from the upper 1 m of the water column; the equivalent turnover rates for NAS*a* would be 8.1 (CH_4 oxidation) and 0.9 days (efflux). Rapid production and diffusion of CH_4 from deeper waters and sediments to the surface waters of the lake would be needed to maintain the CH_4 concentrations above air equilibrium, and seems unlikely to be a limiting factor for methanotrophy in these waters, where inorganic nutrient supply may impose a greater constraint.

Isotopic signatures

The analysis of isotopic signatures of CH_4 and CO_2 in lithalsa lakes showed large variability in their emission sources. The ^{14}C dating of ebullition samples indicated that microbial community in at least one of these lakes has access to an ancient (mid-Holocene) carbon source, probably of the same postglacial origin as in the other lithalsa lakes in the region (Bouchard et al. 2014). The $\Delta^{14}C$ values of CO_2 emitted by ebullition from lake BGR1 varied by a factor of two, with a maximum age of around 6000 years. The $\Delta^{14}C$ values of CH_4 in the same samples from BGR1 also varied by about a factor of two, but corresponded to more modern ages (100 to 320 y BP). This divergence in $\Delta^{14}C$ signatures, with values corresponding to a much older age of the CO_2 carbon vs. that of CH_4, implies at least partial separation of the pathways for production of the two gases. It is important to note however that the CO_2 ebullition flux measured at BGR is only about 4% of CH_4 ebullition flux (about 37% at KWK), so this old carbon source may have a negligible impact in terms of greenhouse effect. Differences in age have been found in other studies in the region and further north in the Canadian Arctic (Bouchard et al. 2015; Matveev et al. 2016; Negandhi et al. 2013), and sometimes with the reverse trend showing older CH_4

associated with methanogenesis based on old organic carbon released from degrading permafrost (Matveev et al. 2016). The older CO_2 measured here could potentially be derived from subsurface flows into the lake that pick up this gas from soil decomposition processes, including from thermokarst organic soils as described in the Alaskan tundra by Kling et al. (1991). Younger CH_4 could be derived from vegetation that occurs at the edge of and within the lithalsa lakes, and that is broken down by anaerobic processes in the bottom waters and sediments. However, the data are limited and will require corroboration with more extensive sampling and analyses.

The analysis of the $\delta^{13}C$ signatures showed a marked difference between the lithalsa lakes in discontinuous permafrost (BGR) versus those in the largely degraded permafrost (KWK). This difference was especially apparent in the bottom waters, which, in most of these lakes, would be little affected by aerobic oxidation of CH_4 that would deplete the $\delta^{13}C$ of the remaining CH_4. More depleted (i.e., more negative) values of $\delta^{13}C$-CH_4 have been attributed to the differential use of lighter substrate carbon by methanogens (Whiticar 1999; Conrad 2005; Sanci and Panarello 2015). This also leads to carbon isotope separation between CH_4 and CO_2, which can indicate the methanogenic pathways that predominate (Whiticar 1999; Galand et al. 2010). In particular, Whiticar (1999) showed that carbon isotope separation factor ε_C (Eq.2) in the range of 40 to 55‰ is most commonly associated with methylated substrate fermentation prevailing in freshwater environments, while higher and lower values were linked to acetoclastic (AM) and hydrogenotrophic (HM) pathways of CH_4 production respectively, with some overlap on both sides (Galand et al. 2010; Penger et al. 2012; Vaughn et al. 2016). The ε_C values observed in the lithalsa lakes mostly fall at the edge between the ranges associated with HM and AM. This is in line with the analysis of archaeal 16S rRNA in these lakes (Crevecoeur et al. 2016), which found methanogens of the orders Methanomicrobiales (hydrogenotrophic) and Methanosarcinales

(multiple pathways) to co-occur in abundance as the dominant Archaea. The lower ε_C values observed in the surface waters of the lithalsa lakes relative to those in the bottom waters (Table 3) could potentially be linked to CH_4 oxidation in the oxygenated epilimnion. The more depleted $\delta^{13}C\text{-}CH_4$ values observed in the bottom of the KWK lakes (Table 5) may be linked to a greater degree of the substrate depletion by the methanogens.

Conclusions

Our subarctic observations indicate that lithalsa lakes begin emitting CH_4 and CO_2 as soon as they are formed. These emissions are through ebullition and diffusion pathways, and are liable to continue and accelerate, particularly via diffusive fluxes, as the permafrost continues to warm and erode. CH_4 oxidation appears to have a variable effect in reducing the stocks and therefore diffusive transfers of this gas to the atmosphere; at NAS the oxidation rates were a factor of ten less than emission rates (11% of the calculated efflux from the upper metre of the water column to the atmosphere), but at KWK the oxidation rates were equivalent to around 63% of emissions, indicating a substantive reduction of potential emission rates by methanotrophy. Despite this effect of CH_4 oxidation, the KWK lakes were stronger emitters of CH_4 than at northern sites, and also emitted more CO_2 per unit area. Detailed surveys of lake sizes and density distributions will be needed to fully extrapolate these findings to the landscape scale. However, if the southern KWK lakes can be considered a space for time proxy for future change (Blois et al. 2013), these observations imply that thermokarst development in the lithalsa dominated landscape will be accompanied by increased GHG emissions, and that the lakes will persist as strong sources for at least many decades.

Acknowledgements

We acknowledge the support of the Centre d'études nordiques (CEN), the Natural Sciences and Engineering Research Council of Canada (NSERC) including the Discovery Frontiers project ADAPT, the Canada Research Chair program, the Canada First Research Excellence Funds program Sentinel North (BOND), the Quebec Nature and Technology Research funds (FRQNT), and the Northern Science Training Program. We also thank Valentin Proult for permission to reproduce the bathymetric data in Fig. S3[1], Tursujuq National Park (Kativik Regional Government) for permission to sample at BGR and NAS, two anonymous reviews for their valuable comments and suggestions, and all of those who helped us in the field and laboratory.

References

Allan, J., Ronholm, J., Mykytczuk, N.C.S., Greer, C.W., Onstott, T.C. and Whyte, L.G. 2014. Methanogen community composition and rates of methane consumption in Canadian High Arctic permafrost soils. Environ. Microbiol. Rep. **6**: 136–144. doi: 10.1111/1758-2229.12139.

Allard, M., and Seguin, M.-K. 1987. Le pergélisol au Québec nordique: bilan et perspectives. Géogr. Phys. Quat. **41**: 141–152. doi:10.7202/032671ar.

APHA, AWWA, and WEF. 1998. American Public Health Association (APHA), American Water Works Association (AWWA), and Water Environment Federation (WEF). 1998. Standard Methods for the Examination of Water and Wastewater 20th Edition. United Book Press, Inc., Baltimore, Maryland.

Bastviken, D., Tranvik, L., Downing, J.A., Crill, P.M., and Enrich-Prast, A. 2011. Freshwater methane emissions offset the continental carbon sink. Science. **331**: 50. doi: 10.1126/science.1196808.

Bégin, P.N., and Vincent, W.F. 2017. Permafrost thaw ponds as habitats for abundant rotifer populations. Arctic Sci. **3**: 354-377. doi: 10.1139/AS-2016-0017.

Bhiry, N., Delwaide, A., Allard, M., Bégin, Y., Filion, L., Lavoie, M., Nozais, C., Payette, S., Pienitz, R., Saulnier-Talbot, É. and Vincent, W.F. 2011. Environmental change in the Great Whale River region, Hudson Bay: Five decades of multidisciplinary research by Centre d'études nordiques (CEN). Ecoscience. **18**: 182–203. doi: 10.2980/18-3-3469.

Blois, J.L., Williams, J.W., Fitzpatrick, M.C., Jackson, S.T., and Ferrier, S. 2013. Space can substitute for time in predicting climate-change effects on biodiversity. Proc. Natl. Acad. Sci. USA. **110**: 9374-9379. doi: 10.1073/pnas.1220228110.

Bogard, M. J., Del Giorgio, P. A., Boutet, L., Chaves, M. C. G., Prairie, Y. T., Merante, A.,et al. 2014. Oxic water column methanogenesis as a major component of aquatic CH_4 fluxes. Nat. Commun. **5**: 5350. doi: 10.1038/ncomms6350.

Bonilla, S., Villeneuve, V., and Vincent, W.F. 2005. Benthic and planktonic algal communities in a High Arctic Lake: pigment structure and contrasting responses to nutrient enrichment. J. Phycol. **41**: 1120–1130. doi: 10.1111/j.1529- 8817.2005.00154.x.

Bouchard, F., Francus, P., Pienitz, R., Laurion, I., and Feyte, S. 2014. Subarctic thermokarst ponds: Investigating recent landscape evolution and sediment dynamics in thawed permafrost of northern Québec (Canada). Arct. Antarct. Alp. Res. **46**: 251–271. doi: 10.1657/1938-4246-46.1.251.

Bouchard, F., Laurion, I., Prieskienis, V., Fortier, D., Xu, X., and Whiticar, M.J. 2015. Modern to millennium-old greenhouse gases emitted from ponds and lakes of the Eastern Canadian

Arctic (Bylot Island, Nunavut). Biogeosci. **12**: 7279–7298. doi: 10.5194/bg–12-7279-2015.

Bouchard, F., MacDonald, L.A., Turner, K.W., Thienpont, J.R., Medeiros, A.S., Biskaborn, B.K., Korosi, J., Hall, R.I., Pienitz, R., and Wolfe, B.B. 2016. Paleolimnology of thermokarst lakes: a window into permafrost landscape evolution. Arctic Sci. **3**: 91–117. doi:10.1139/as-2016-0022.

Breton, J., Vallieres, C., and Laurion, I. 2009. Limnological properties of permafrost thaw ponds in northeastern Canada. Can. J. Fish. Aquat. Sci. **66**: 1635–1648. doi:10.1139/F09–108.

Calmels, F., Allard, M., and Delisle, G. 2008. Development and decay of a lithalsa in northern Quebec: a geomorphological history. Geomorphology **97**: 287–299. doi: 10.1016/j.geomorph.2007.08.013.

Carignan, R. 1998. Automated determination of carbon dioxide, oxygen, and nitrogen partial pressures in surface waters. Limnol. Oceanogr. **43**: 969–975. doi: 10.4319/lo.1998.43.5.0969.

Casper, P., Maberly, S.C., Hall, G.H., and Finlay, B. J. 2000. Fluxes of methane and carbon dioxide from a small productive lake to the atmosphere. Biogeochem. **49**: 1–19. doi:10.1023/A:1006269900174.

Conrad, R. 2005. Quantification of methanogenic pathways using stable carbon isotopic signatures: a review and a proposal. Org. Geochem. **36**: 739–752. doi: 10.1016/j.orggeochem.2004.09.006

Coplen, T.B. 2011. Guidelines and recommended terms for expression of stable-isotope-ratio and gas-ratio measurement results. Rapid Commun. Mass Spectrom. **25**: 2538–2560. doi: 10.1002/rcm.5129.

Crevecoeur, S., Vincent, W.F., Comte, J., and Lovejoy, C. 2015. Bacterial community structure across environmental gradients in permafrost thaw ponds: Methanotroph-rich ecosystems. Front. Microbiol. **6**: 192. doi: 10.3389/fmicb.2015.00192.

Crevecoeur, S., Vincent, W.F., and Lovejoy, C. 2016. Environmental selection of planktonic methanogens in permafrost thaw ponds. Sci. Rep. **6**: 31312. doi: 10.1038/srep31312.

Deshpande, B.N., MacIntyre, S., Matveev, A., and Vincent, W.F. 2015. Oxygen dynamics in permafrost thaw lakes: Anaerobic bioreactors in the Canadian subarctic. Limnol. Oceanogr. **60**: 1656–1670. doi: 10.1002/lno.10126.

Deshpande, B.N., Crevecoeur, S., Matveev, A. and Vincent, W.F. 2016. Bacterial production in subarctic peatland lakes enriched by thawing permafrost. Biogeosci. 13: 4411–4427. doi: 10.5194/bg–13-4411-2016.

Deshpande, B.N., Maps, F., Matveev, A., and Vincent, W.F. 2017. Oxygen depletion in subarctic peatland thaw lakes. Arctic Sci. **3:** 406-428. doi: 10.1139/AS-2016-0048.

578 Elvert, M., Pohlman, J.W., Becker, K.W., Gaglioti, B., Hinrichs, K.-U., and Wooller, M.J. 2016.
579 Methane turnover and environmental change from holocene lipid biomarker records in a
580 thermokarst lake in arctic Alaska. Holocene. **26**: 1766–1777. doi:
581 10.1177/0959683616645942.

582 Emmerton, C. A., St. Louis, V. L., Lehnherr, Graydon, J. A., Kirk, J. L., and K. J. Rondeau.
583 2016. The importance of freshwater systems to the net atmospheric exchange of carbon
584 dioxide and methane with a rapidly changing High Arctic watershed. Biogeosci. **13**:
585 5849–5863. doi: 10.5194/bg–13-5849-2016.

586 Galand, P.E., Yrjälä, K., Conrad, R. 2010. Stable carbon isotope fractionation during
587 methanogenesis in three boreal peatland ecosystems. Biogeosci. **7**: 3893–3900. doi:
588 10.1111/gcb.13281.

589 Grosse, G., Jones, B., and Arp, C. 2013. 8.21 Thermokarst lakes, drainage, and drained basins. *In*
590 Treatise on Geomorphology. Edited by J.F. Shroder. pp. 325–353. Academic Press, San
591 Diego. doi: 10.1016/B978-0–12-374739-6.00216-5.

592 Grosse, G., Goetz, S., McGuire, A.D., Romanovsky, V.E., and Schuur, E.A.G. 2016. Changing
593 permafrost in a warming world and feedbacks to the Earth system. Environ. Res. Lett. **11**:
594 040201. doi: 10.1088/1748-9326/11/4/040201.

595 He, R., Wooller, M.J., Pohlman, J.W., Quensen, J., Tiedje, J.M., Leigh, M.B. 2012. Shifts in
596 identity and activity of methanotrophs in Arctic lake sediments in response to temperature
597 changes. Appl. Environ. Microbiol. **78**: 4715– 4723. doi: 10.1128/AEM.00853–12.

598 Holgerson, M.A., and Raymond, P.A. 2016. Large contribution to inland water CO_2 and CH_4
599 emissions from very small ponds. Nature Geosci. **9**: 222-226. doi: 10.1038/ngeo2654.

600 Huttunen, J.T., Alm, J., Liikanen, A., Juutinen, S., Larmola, T., Hammar, T., Silvola, J., and
601 Martikainen, P.J. 2003. Fluxes of methane, carbon dioxide and nitrous oxide in boreal
602 lakes and potential anthropogenic effects on the aquatic greenhouse gas emissions.
603 Chemosphere. **52**: 609–621. doi: 10.1016/S0045-6535(03)00243–1.

604 Kanevskiy, M., Jorgenson, T., Shur, Y., O'Donnell, J.A., Harden, J.W., Zhuang, Q., and Fortier,
605 D. 2014. Cryostratigraphy and permafrost evolution in the lacustrine lowlands of west-
606 central Alaska. Permafr. Periglac. Process. **25**: 14–34. doi: 10.1002/ppp.1800.

607 Kankaala, P., Huotari, J., Peltomaa, E., Saloranta, T., and Ojala, A. 2006. Methanotrophic activity
608 in relation to methane efflux and total heterotrophic bacterial production in a stratified,
609 humic, boreal lake. Limnol. Oceanogr. **51**: 1195–1204. doi: 10.4319/lo.2006.51.2.1195.

610 Kling, G. W., Kipphut, G.W., and Miller, M. C. 1991. Arctic lakes and streams as gas conduits to
611 the atmosphere: implications for tundra carbon budgets. Science **251**: 298-301. doi:
612 10.1126/science.251.4991.298.

613 Kokelj, S.V., and Jorgenson, M.T. 2013. Advances in thermokarst research. Permafrost
614 Periglacial Process. **24**: 108–119. doi:10.1002/ppp.1779.

615 Laurion, I., Vincent, W.F., MacIntyre, S., Retamal, L., Dupont, C., Francus, P., and Pienitz, R.
616 2010. Variability in greenhouse gas emissions from permafrost thaw ponds. Limnol.
617 Oceanogr. **55**: 115–133. doi: 10.4319/lo.2010.55.1.0115.

618 Lindgren, P.R., Grosse, G., Walter Anthony, K.M., and Meyer, F.J. 2016. Detection and
619 spatiotemporal analysis of methane ebullition on thermokarst lake ice using high-
620 resolution optical aerial imagery. Biogeosci. **13**: 27–44. doi: 10.5194/bgd–12-7449-2015.

621 Lipson, D.A., Raab, T.K., Parker, M., Kelley, S.T., Brislawn, C.J., and Jansson, J. 2015. Changes
622 in microbial communities along redox gradients in polygonized Arctic wet tundra soils,
623 Environ. Microbiol. Rep. **7**: 649–657. doi: 10.1111/1758-2229.12301.

624 Martinez-Cruz, K., Sepulveda-Jauregui, A., Walter Anthony, K., and Thalasso, F. 2015.
625 Geographic and seasonal variation of dissolved methane and aerobic methane oxidation in
626 Alaskan lakes. Biogeosc. **12**: 4595-4606. doi: 10.5194/bg–12-4595-2015.

627 Matveev, A., Laurion, I., Deshpande, B.N., Bhiry, N., and Vincent, W.F. 2016. High methane
628 emissions from thermokarst lakes in subarctic peatlands. Limnol. Oceanogr. **61**(S1):
629 S150-S164. doi: 10.1002/lno.10311.

630 Myhre, G., Shindell, D., Bréon, F.-M., Collins, W., Fuglestvedt, J. , Huang, J. , Koch, D.,
631 Lamarque, J.-F. , Lee, D., Mendoza, B., Nakajima, T., Robock, A., Stephens, G.,
632 Takemura T., and Zhang, H. 2013. Anthropogenic and Natural Radiative Forcing. *In*
633 Climate Change 2013: The Physical Science Basis. Contribution of Working Group I to
634 the Fifth Assessment Report of the Intergovernmental Panel on Climate Change. *Edited*
635 *by* T.F. Stocker, D. Qin, G.-K. Plattner, M. Tignor, S.K. Allen, J. Boschung, A. Nauels,
636 Y. Xia, V. Bex and P.M. Midgley. Cambridge University Press, Cambridge, United
637 Kingdom and New York, NY, USA.

638 Negandhi, K., Laurion, I., Whiticar, M.J., Galand, P.E., Xu, X., and Lovejoy, C. 2013. Small
639 thaw ponds: An unaccounted source of methane in the Canadian High Arctic. PLoS ONE.
640 **8**: e78204. doi: 10.1371/journal.pone.0078204.

641 Payette, S., Delwaide, A., Caccianiga, M., and Beauchemin, M. 2004. Accelerated thawing of
642 subarctic peatland permafrost over the last 50 years. Geophys. Res. Lett. **31**: L18208. doi:
643 10.1029/2004GL020358.

644 Penger, J., Conrad, R., Blaser, M. 2012. Stable carbon isotope fractionation by methylotrophic
645 methanogenic archaea. Appl. Environ. Microbiol. **78**: 7596–7602. doi:
646 10.1128/AEM.01773–12

647 Pienitz, R., Bouchard, F., Narancic, B., Vincent, W.F., and Sarrazin, D. 2016. Seasonal ice cover
648 and catchment changes at northern thermokarst ponds in Nunavik: Observations from
649 automated time-lapse cameras, v. 1.0 (2014-2015). Nordicana. **D24**. doi:
650 10.5885/45418AD-AF6A8064C702444B.

651 Prairie Y.T., and del Giorgio, P.A. 2013. A new pathway of freshwater methane emissions and
652 the putative importance of microbubbles. Inland Waters. **3**: 311–320. doi: 10.5268/IW-
653 3.3.542.

654 Proult, V. 2014. L'origine périglaciaire et son influence sur les écosytèmes thermokarstiques au
655 Nunavik: Analyse des communautés d'algues silicieuses. M. Sc. Thesis. Université Laval,
656 225 pp.

657 Repo, M. E., Huttunen, J. T., Naumov, A. V., Chichulin, A. V., Lapshina, E. D.,, Bleuten, W.,
658 and Martikainen, P. J. 2007. Release of CO_2 and CH_4 from small wetland lakes in
659 western Siberia. Tellus Ser. B. **59**: 788–796. doi: 10.1111/j.1600-0889.2007.00301.x.

660 Roiha, T., Laurion, I., and Rautio, M. 2015. Carbon dynamics in highly heterotrophic subarctic
661 thaw ponds. Biogeosci. **12**: 7223–7237. doi: 10.5194/bg–12-7223-2015.

662 Sanci, R. and Panarello, H. 2015. Carbon and hydrogen isotopes as tracers of methane dynamic in
663 wetlands. Int. J. Geosci. **6**: 720-728. doi: 10.4236/ijg.2015.67058.

664 Sepulveda-Jauregui, A., Walter Anthony, K.M., Martinez-Cruz, K., Greene, S., and Thalasso, F.
665 2015. Methane and carbon dioxide emissions from 40 lakes along a north–south
666 latitudinal transect in Alaska. Biogeosci. **12**: 3197–3223. doi: 10.5194/bg–12-3197-2015.

667 Stuiver, M., and Polach, H.A. 1977. Discussion: reporting of 14C data. Radiocarbon **19**: 355–
668 363. doi: 10.1017/S0033822200003672.

669 Tan, Z., and Zhuang, Q. 2015. Arctic lakes are continuous methane sources to the atmosphere
670 under warming conditions. Environ. Res. Lett. **10**: 054016. doi: 10.1088/1748-
671 9326/10/5/054016.

672 Vachon, D., Prairie, Y.T., and Cole, J.J. 2010. The relationship between near-surface turbulence
673 and gas transfer velocity in freshwater systems and its implications for floating chamber
674 measurements of gas exchange. Limnol. Oceanogr. **55:** 1723–1732. doi:
675 10.4319/lo.2010.55.4.1723.

676 Vallée, S., and Payette, S. 2007. Collapse of permafrost mounds along a subarctic river over the
677 last 100 years (northern Québec). Geomorphology. **90:** 162–170. doi:
678 10.1016/j.geomorph.2007.01.019.

679 van Huissteden, J., Berrittella, C., Parmentier, F.J.W., Mi, Y., Maximov, T.C., and Dolman, A.J.
680 2011. Methane emissions from permafrost thaw lakes limited by lake drainage. Nat. Clim.
681 Change. **1**: 119–123. doi: 10.1038/ nclimate1101.

682 Vaughn, L.J.S., Conrad, M.E., Bill, M. and Torn, M.S. 2016. Isotopic insights into methane
683 production, oxidation, and emissions in Arctic polygon tundra. Glob Change Biol. **22**:
684 3487–3502. doi: 10.1111/gcb.13281.

685 Vincent, W.F., Lemay, M., and Allard, M. 2017. Arctic permafrost landscapes in transition:
686 Towards an integrated Earth system approach. Arctic Sci. **3**: 39-64. doi: 10.1139/AS-
687 2016-0027.

688 Walter, K.M., Zimov, S.A., Chanton, J.P., Verbyla, D., and Chapin, F.S. 2006. Methane bubbling
689 from Siberian thaw lakes as a positive feedback to climate warming. Nature. **443**: 71–75.
690 doi: 10.1038/nature05040.

691 Walter Anthony K., and MacIntyre, S. 2016. Biogeochemistry: Nocturnal escape route for marsh
692 gas. 2016. Nature. **535**: 363. doi: 0.1038/535363a.

693 Walter Anthony, K.M., Vas, D.A., Brosius, L., Chapin III, F.S., Zimov, S.A., and Zhuang, Q.
694 2010. Estimating methane emissions from northern lakes using ice-bubble surveys.
695 Limnol. Oceanogr. Methods **8**: 592–609. doi: 10.4319/lom.2010.8.0592.

696 Watanabe, S. Laurion, I., Pienitz, R., Chokmani, K., and Vincent, W.F. 2011. Optical diversity of
697 thaw lakes in discontinuous permafrost: A model system for water color analysis. J.
698 Geophys. Res. – Biogeosc. **116**: G02003. doi:10.1029/2010JG001380.

699 Whiticar, M.J. 1999. Carbon and hydrogen isotope systematics of bacterial formation and
700 oxidation of methane. Chem. Geol. **161**: 291–314. doi: 10.1016/S0009-2541(99)00092-3.

701 Wik, M., Crill, P.M., Bastviken, D., Danielsson, Å., and Norbäck, E. 2011. Bubbles trapped in
702 arctic lake ice: Potential implications for methane emissions. J. Geophys. Res. **116**:
703 G03044. doi: 10.1029/2011JG001761.

704 Wik, M., Crill, P.M., Varner, R.K., and Bastviken D. 2013. Multiyear measurements of ebullitive
705 methane flux from three subarctic lakes. J. Geophys. Res. Biogeosci. **118**: 1307–1321,
706 doi: 10.1002/jgrg.20103.

707 Wik, M., Varner, R.K., Walter Anthony, K., MacIntyre, S., and Bastviken, D. 2016. Climate-
708 sensitive northern lakes and ponds are critical components of methane release. Nature
709 Geosci. **9:** 99–105. doi: 10.1038/ngeo2578.

710 Zimov, S.A., Voropaev, Y.V., Semiletov, I.P., Davidov, S.P., Prosiannikov, S.F., Chapin III, F.S.,
711 Chapin, M.C., Trumbore, S., and Tyler, S. 1997. North Siberian lakes: A methane source
712 fueled by Pleistocene carbon. Science. **277:** 800–802. doi:10.1126/science.277.5327.800.

713

Tables

Table 1. Biogeochemical properties of the studied lakes, including total nitrogen (TN), total phosphorus (TP), soluble reactive phosphorus (SRP), chlorophyll *a* (Chl-*a*), total suspended solids (TSS), dissolved organic carbon (DOC), and dissolved CO_2 and CH_4 concentrations.

Lake	TN (mg N L^{-1})	TP (mg P L^{-1})	SRP (µg P L^{-1})	Chl-*a* (µg L^{-1})	TSS (mg L^{-1})	DOC (mgC L^{-1})	CO_2 (µmol L^{-1})	CH_4 (µmol L^{-1})
Surface								
KWK1	1.08	0.47	5.0	8.7	14	17	32	0.1
KWK11	1.01	0.12	< 3	24	8.3	27	42	0.13
KWK12	0.41	0.02	0.4	5.6	2.4	6.3	44	0.9
BGR1	0.24	0.01	0.4	1.0	2.0	2.4	30	0.8
BGR2	0.43	0.04	3.3	0.9	5.9	10	20	0.5
BGR*b*	0.11	0.01	4.1	-	10	4.1	43	0.4
NAS*a*	4.22	0.13	2.9	3.0	319	3.0	15	0.13
NAS*h*	0.60	0.03	6.2	3.6	18	4.1	30	0.19
Bottom								
KWK1	0.94	0.05	11	19	188	12	807	190
KWK11	0.57	0.02	< 3	39	27	18	731	40
KWK12	0.63	0.07	1.8	5	6	8	762	710
BGR1	0.51	0.06	2.1	4.6	14	3	382	197
BGR2	-	-	-	-	31	10	193	3
NAS*a*	4.14	0.18	19	2	810	2	97	0.02

721 **Table 2**. Average (summer 2012-2015) surface CH_4 and CO_2 concentrations per study site.
722

Gas concentration		Study site		
		NAS	BGR	KWK
CO_2 surface				
Mean	(µmol L^{-1})	23.6	33.0	45.5
Coefficient of variation	(%)	40	25	25
Number of measurements	(n)	12	11	8
CH_4 surface				
Mean	(µmol L^{-1})	0.15	0.41	0.43
Coefficient of variation	(%)	44	54	78
Number of measurements	(n)	12	11	8

723
724

725 **Table 3**. Average (summer 2012-2015) CO_2 and CH_4 flux (diffusion and ebullition) and their
726 greenhouse gas forcing per study site (given as CO_2-equivalent[†]). Yearly estimates are for the
727 open water period, as determined from the automated camera images.

Gas flux		Study site		
		NAS	BGR	KWK
CO_2 ebullition				
Mean rate	(mmol m^{-2} d^{-1})	–	0.01	0.006
	(mg CO_2 m^{-2} d^{-1})	–	0.4	0.26
Coefficient of variation	(%)	–	132	116
Number of measurements	(n)	–	2	2
CO_2 diffusion				
Mean rate	(mmol m^{-2} d^{-1})	3.4	8.1	20.2
	(mg CO_2 m^{-2} d^{-1})	150	357	889
Coefficient of variation	(%)	169	95	35
Number of measurements	(n)	6	6	6
CH_4 ebullition				
Mean rate	(mmol m^{-2} d^{-1})	–	0.26	0.016
	(mg CO_2-eq m^{-2} d^{-1})[†]	–	117	7
Coefficient of variation	(%)	–	136	132
Number of measurements	(n)	–	2	2
CH_4 diffusion				
Mean rate	(mmol m^{-2} d^{-1})	0.12	0.45	0.47
	(mg CO_2-eq m^{-2} d^{-1})	54	202	211
Coefficient of variation	(%)	25	12	70
Number of measurements	(n)	6	6	6
Total greenhouse gas forcing				
	(mg CO_2-eq m^{-2} d^{-1})	204*	676	1108
Average lake area	(m^2)	2035	728	427
Open water period	(days)	133	134	145
per lake per open water period	(kg CO_2-eq y^{-1})	55*	66	68

* diffusion only

[†] For methane, CO_2-equivalent (CO_2-eq.) = CH_4 (mg CH_4 m^{-2} d^{-1}) x 28, to consider its global warming potential over 100 years, as in Myhre et al. (2013).

728

729 **Table 4**. The diffusive and ebullition flux of CH_4 and CO_2 from lithalsa lakes (2012-2015
730 average) compared with other lakes in the circumpolar region.

Site [Ref.*]		Canada				Finland	Alaska	Siberia
		Lithalsa (mineral) [1]	Palsa (peatland) [2]	Tundra lakes [3]	High Arctic [4]	Permafrost boreal [5]	Continuous yedoma [6]	Tundra (peatland)[7]
Latitude (ºN)		55-57	55-57	73	82	61.5	60-68	65
CH_4 ebullition								
(mmol m^{-2} d^{-1})	Mean rate	0.1	0.2	16.9	0.001	0.9	5.5	0.2
	Range	0.02-0.25	<0.01-0.8	0.00-535	0.00-0.01	0.2–1.5	2.2-7.2	0.04-0.3
CH_4 diffusion								
(mmol m^{-2} d^{-1})	Mean rate	0.4	3.3	0.8	0.7	0.7	0.9	0.4
	Range	0.07-0.82	0.01–12.8	0.03-5.8	0.00–1.34	0.1-2.0	0.6–1.1	0.2-0.6
CO_2 ebullition								
(mmol m^{-2} d^{-1})	Mean rate	0.1	0.01	0.7	0.002	0.3	0.11	0.005
	Range	0.006-0.2	0.001-0.1	0.00–16.3	0.00-0.01	0.002-0.5	0.01-0.14	0-0.03
CO_2 diffusion								
(mmol m^{-2} d^{-1})	Mean rate	12.3	58.3	8.7	7.2	17.0	133.9	34.1
	Range	–1.7-30.8	4-242	–12-65	0.00–165	9-25	4.6-263	11.4-59

731 *References in the table: [1] This study, [2] Matveev et al. 2016, [3] Bouchard et al. 2015, [4] Emmerton et al.
732 2016, [5] Huttunen et al. 2003, [6] Sepulveda-Jauregui et al. 2015, [7] Repo et al. 2007.

733

734 **Table 5**. Isotopic fractionation $\delta^{13}C$ of CH_4 and CO_2 dissolved in surface and bottom waters at
735 KWK and BGR sites (Aug 2015), and the separation factor ε_C in these lakes ($\delta^{13}C$ vs. VPDB,
736 mean ±SD, n=3).

Lake	$\delta^{13}C$-CH_4 (±SD) ‰	$\delta^{13}C$-CO_2 (±SD) ‰	ε_C ‰
Surface			
KWK1	-45.7 (0.5)	–14.8 (0.3)	30.9
KWK11	-46.2 (0.0)	–16.2 (0.0)	30.0
KWK12	-47.0 (0.1)	–14.2 (0.3)	32.8
Average	-46.3 (0.2)	–15.1 (0.2)	31.2
Bottom			
KWK1	-66.1 (0.0)	–17.4 (0.0)	48.7
KWK11	-56.6 (0.8)	–18.1 (0.5)	38.4
KWK12	-67.0 (1.6)	-22.3 (1.7)	44.8
Average	-63.2 (0.8)	–19.3 (0.7)	44.0
Surface			
BGR1	-47.9 (0.5)	–13.8 (1.3)	34.1
BGR2	-48.2 (4.1)	–16.1 (2.7)	32.1
BGR*b*	-30.7 (0.3)	–15.8 (0.3)	14.9
Average	-42.3 (1.6)	–15.2 (1.4)	27.1
Bottom			
BGR1	-55.2 (3.7)	–13.6 (1.8)	41.6
BGR2	-47.1 (0.2)	–17.7 (1.0)	29.4
BGR*b*	-51.8 (0.7)	–12.1 (1.7)	39.7
Average	-51.4 (1.5)	–14.5 (1.5)	36.9

737

738 **Figure legends**
739
740 **Fig. 1.** Study region and permafrost distribution in Nunavik (QC, Canada). The studied sites
741 NAS, BGR and KWK are indicated as black dots on the eastern shore of the Hudson Bay.
742 Permafrost types in the region of study (A*llard and Seguin* 1987) are shown with each type
743 separated by dashed lines, where C, E, S, and I indicate the zones of continuous permafrost (C,
744 90–100% of land area underlain by permafrost), discontinuous extended (E, 50–90%),
745 discontinuous sporadic (S, 10–50%), and isolated patches of permafrost (I, 0–10%).
746
747 **Fig. 2.** Morphological changes at the BGR site from 2010 to 2012, seen at oblique aerial
748 photographs made with a 2-year interval, showing permafrost degradation (thermokarst process).
749 New thermokarst lakes were formed (1, 3). The existing lithalsa lakes, including the studied lakes
750 BGR1 and BGR2 (2), increased in surface area or merged with adjacent water bodies (4). The
751 reference scale on the images is approximate.
752
753 **Fig. 3.** Vertical profiles of the measured physical, chemical and biological characteristics in one
754 representative lake from each of the three study sites located in the discontinuous widespread
755 (NASa; top panels), discontinuous (BGR1; middle panels), and sporadic (KWK12; bottom
756 panels) permafrost (data from August 2014 shown).
757
758 **Fig. 4.** Gas concentration profiles in representative lakes from each of the three study sites
759 located in the discontinuous widespread (NAS profiles from 7 August 2012), discontinuous
760 (BGR profiles from 9 August 2012), and sporadic (KWK profiles from 25 August 2015)
761 permafrost.
762
763 **Fig. 5.** Surface and bottom CH_4 and CO_2 concentrations at the northernmost (NAS) and
764 southernmost (KWK) sites (average for summer observations from 2012 to 2015).
765
766 **Fig. 6.** Dissolved gas concentrations measured along the South-North transect crossing lake
767 NAS*a* on 24 August 2014 at the surface and at 1 m depth. The bottom panel shows the
768 bathymetry and corresponding stations on the lake.
769
770 **Fig. 7.** Isotopic fractionation $\delta^{13}C$ of CO_2 and CH_4 in surface and bottom waters of the lakes
771 sampled at KWK and BGR sites, and the separation factor ε_C in these lakes (data from August
772 2015).
773
774 **Fig. 8.** The concurrent CH_4 oxidation and CO_2 accumulation rates in lake water sampled from
775 NAS*a* and KWK12, estimated as linear regressions of dissolved gas concentrations (data from
776 August 2014) measured every 3 h in the water incubated for 27 to 48 hours.
777

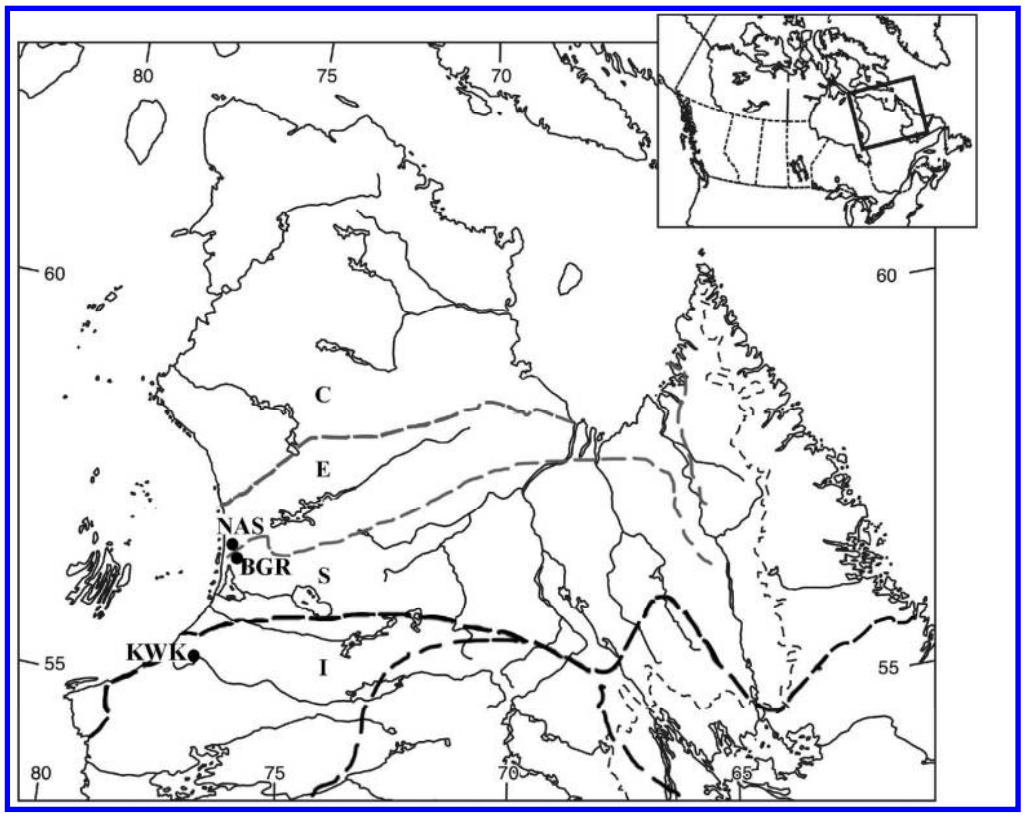

Fig. 1. Study region and permafrost distribution in Nunavik (QC, Canada). The studied sites NAS, BGR and KWK are indicated as black dots on the eastern shore of the Hudson Bay. Permafrost types in the region of study (Allard and Seguin 1987) are shown with each type separated by dashed lines, where C, E, S, and I indicate the zones of continuous permafrost (C, 90–100% of land area underlain by permafrost), discontinuous extended (E, 50–90%), discontinuous sporadic (S, 10–50%), and isolated patches of permafrost (I, 0–10%).

190x151mm (300 x 300 DPI)